On Band-stitching for Wideband Vector Measurements With Vector Signal Analyzers

Ji, Yilin; Nielsen, Jesper Ødum; Fan, Wei

Published in:
I E E E Transactions on Microwave Theory and Techniques

DOI (link to publication from Publisher):
10.1109/TMTT.2022.3207997

Publication date:
2023

Document Version
Accepted author manuscript, peer reviewed version

On Band-stitching for Wideband Vector Measurements With Vector Signal Analyzers

Yilin Ji, Jesper Ødum Nielsen, and Wei Fan

***Abstract*—As the bandwidth of radio signals increases significantly over the evolution of communication systems, the analysis bandwidth of many current instruments becomes insufficient. In this paper, we study analysis bandwidth extension using the so-called band-stitching. Specifically, we propose a two-step delay estimation method which combines the cross-correlation and an additional refining step to resolve the timing impairment between different sampling branches in post-processing. We verify the method with a sequential measurement setup, using vector signal analyzers (VSAs). The result shows the necessity of conducting the refining step for getting a more accurate delay estimate to successfully recover the original wideband signal. Besides, a good agreement is found between the stitched data and the reference data in terms of the waveforms and error vector magnitude (EVM), which shows the effectiveness and robustness of the proposed calibration method in practice.**

***Index Terms*—Band-stitching, EVM measurements, and sub-band impairment correction.**

I. Introduction

The emerging fifth-generation (5G) new radio (NR) has a much wider bandwidth compared to the previous fourth-generation (4G) long term evolution (LTE). It is stated in the standard [1] of the 3rd Generation Partnership Project (3GPP) that each carrier of the 5G NR signal in the frequency range 2 (FR2) could occupy a bandwidth of up to 400 MHz per carrier, whereas 4G LTE occupies up to only 20 MHz bandwidth per carrier. The wider bandwidth greatly increases the throughput of communication systems but, on the other hand, also poses a challenge to measurement instrumentation for the development or testing.

In the case of vector measurements, such as waveform or demodulation measurements, the analysis bandwidth of the instrument needs to be larger than the input signal bandwidth. However, as the bandwidth of signals increases significantly along the evolution of communication systems, the analysis bandwidth of many existing commercial instruments becomes insufficient. To address this problem, besides developing new instruments with a much wider bandwidth, which is time-consuming and expensive, measurement bandwidth extension techniques have been proposed in the literature [2]–[10], which allow instruments of insufficient bandwidth to be used again without hardware modification. Those techniques can be divided into two groups, i.e., time-interleaved methods [2], [3] and frequency-interleaved methods [4]–[10]. In this paper, we study the latter one whose fundamental principle is band-stitching. This principle has also been widely used in other applications when bandwidth extension is considered, such as channel sounding [11], channel emulation [12]–[14], and signal generation [15].

The general procedure of band-stitching for vector measurements involves several steps as follows: 1) spectrum division, 2) sub-band sampling, 3) interpolation and mixing, 4) sub-band impairments calibration, and 5) sub-band stitching. Depending on whether the spectrum division and sub-band sampling are done sequentially or simultaneously for all sub-bands, the practical measurement setup can be configured in a sequential structure [5], [6], [9] or a parallel structure [7], [8], respectively. Due to the fact that different sub-band data are essentially recorded separately either in time (the sequential case) or at different branches (the parallel case), there might exist timing, magnitude, and initial phase impairments among recorded sub-band data. Detailed causes of these impairments are discussed later.

An accurate estimate of the sub-band impairments is of key importance to recover the original signal. In the literature [10], the timing impairment was estimated analytically with a limitation of the input signal being a predefined multisine signal. For more general input signals, the timing correction is mostly resolved through either circular cross-correlation or trigger signals among different sampling branches [5]–[9]. However, those methods are not sufficient to reach an accurate estimate for the timing impairment. Detailed reasons and examples are shown later. Therefore, there is a need for estimation methods of a higher accuracy.

In this paper, we discuss both the sequential and the parallel setup with vector signal analyzers (VSAs). The pros and cons of both setups are given. For the timing correction, we propose a two-step delay estimation method which combines the common circular cross-correlation and an additional refining step. Two series of validation measurement are presented for the sequential setup at 1 GHz and 28 GHz center frequency, respectively. In the measurement, the test signal is set to an orthogonal frequency-division multiplexing (OFDM) NR-FR1-TM3.1a [16] signal. The necessity of conducting the additional refining step is demonstrated. Moreover, the conformity of the stitched signal to the original input signal is evaluated through the comparison of their waveforms and error vector magnitude (EVM).

The main novelty of this work is a two-step delay estimation method to resolve the timing impairment among sub-bands,

This work was supported in part by Innovation Fund Denmark under Project 1046-00006, in part by European 21NRM03 MEWS Projects, and in part by Huawei Technology.

The authors are with the Antenna Propagation and Millimeter-wave Systems (APMS) section at Department of Electronic Systems, Aalborg University, Denmark. Email: {yilin, jni, wfa}@es.aau.dk. (Corresponding author: Wei Fan)

which provides a higher accuracy than just cross-correlation and triggering, and hence allows for analyzing signals of wider bandwidth. The proposed method is examined for stitching with different numbers of sub-bands. Besides, we also show the whole process of the band-stitching for demodulation testing in practice.

The structure of the rest of the paper is given as follows: Section II describes the sequential and the parallel setups, and the principle of band-stitching. Section III elaborates the sub-band impairment correction procedure with a focus on the proposed two-step timing impairment estimation method. Section IV shows the validation measurements and discussion on the results. Lastly, Section V concludes the paper.

II. Setups and Planning

A. Sequential and parallel setups

The sequential setup given in Fig. 1(a) requires only one VSA in the measurement. The transmission of the signal source and the reception of the VSA are controlled by a common trigger signal. The signal source replays the input signal from the beginning every time when a trigger event occurs. Suppose the spectrum of the input signal is divided to N sub-bands. During the nth trigger event, the center frequency of the VSA, f_n, is set to the center frequency of the nth sub-band. The in-phase and quadrature (I/Q) data of that sub-band is recorded.

The parallel setup given in Fig. 1(b) consists of multiple VSAs conducting parallel recording simultaneously. The number of VSAs equals the number of sub-bands. The reception of all VSAs is controlled by a common trigger signal. The center frequency of the VSA at the nth sampling branch, f_n, is set to that of the nth sub-band. Only one trigger event is needed to capture the I/Q data of all sub-bands, since different sub-bands are recorded at their respective sampling branches at the same time.

It is recommended, if possible, to lock the VSAs and signal source to the same reference frequency, e.g., through a 10 MHz signal, to minimize any carrier frequency offset for both setups. Otherwise, carrier recovery may be needed for each sub-band. Similar care could be taken for the sampling clock synchronization among the instruments to minimize any sampling frequency offset.

Compared to the parallel setup, the sequential setup has the advantage of a much lower system cost since only one VSA is involved for the measurement. However, due to its repetitive nature of measurement, it takes N times longer measurement time than the parallel setup to record a signal of the same length. Besides, due to the same reason, the sequential setup cannot handle non-repeatable input signals, e.g., live (cellular) network signals. On the other hand, since different different lengths of sampling paths and triggering paths are involved for the parallel setup, more significant timing impairments among the sub-band measurements are expected to occur.

B. Planning of sub-band division

In the process of the I/Q recording of the VSA, the input signal is first filtered by the analysis filter of the VSA before recording [17]. The analysis filter is an effective filter that

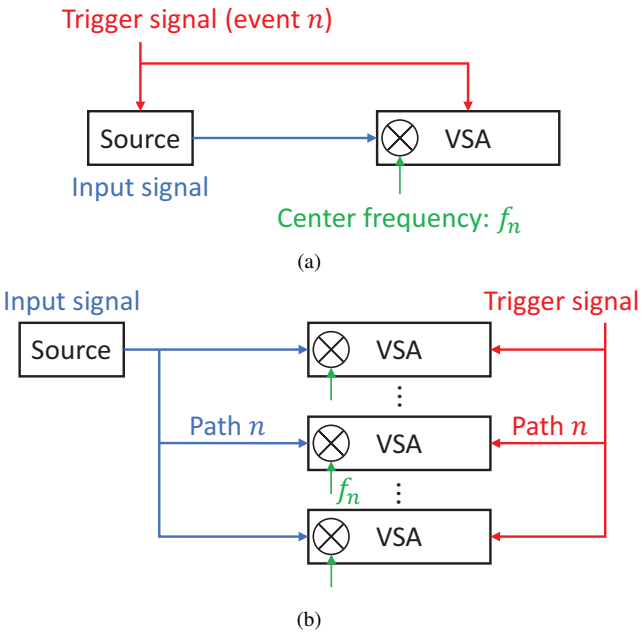

Fig. 1. Diagrams of (a) the sequential setup and (b) the parallel setup. The center frequency of the VSA of the nth trigger event or the nth sampling branch is denoted as f_n.

describes the total effect of all filtering, e.g., at the intermediate-frequency (IF) analog filter, the anti-aliasing filter, etc., that the VSA does before outputting the I/Q data. The bandwidth of the analysis filter, B_{analysis}, which is often referred to as the analysis bandwidth in instrument manuals [17], determines the bandwidth within which the spectrum of the raw input signal can be recorded approximately without distortion, i.e., $H_{\text{analysis}}(f) \approx 1$ within the analysis bandwidth. The value of the analysis bandwidth is usually scaled to the sampling rate of the VSA by a factor of 0.8 [17]. For instance, if the sampling rate were set to 100 MHz, the corresponding analysis bandwidth would be 80 MHz.

A diagram of the relations of the individual sub-bands and the total stitched band is shown in Fig. 2. In the diagram, all sub-bands are of the same analysis bandwidth B_{analysis}. The spacing between the center frequencies of the adjacent sub-bands is Δf for all sub-bands. The overlap bandwidth between the adjacent sub-bands can be found to be

$$B_{\text{overlap}} = B_{\text{analysis}} - \Delta f. \tag{1}$$

The total stitched bandwidth can be found to be

$$B_{\text{stitch}} = (N-1) \cdot \Delta f + B_{\text{analysis}}. \tag{2}$$

Desired values of B_{overlap} and B_{stitch} can be achieved by varying the values of the three variables, i.e., N, Δf, and B_{analysis} when planning for the sub-band division.

III. Sub-band Impairment Correction

For the ease of illustration, the impairment estimation is discussed with a two-band stitching scenario. All three types of impairments are estimated with the recorded sub-band I/Q signals in the overlap band. We assume that when there is no impairment, the signals of adjacent sub-bands in the overlap

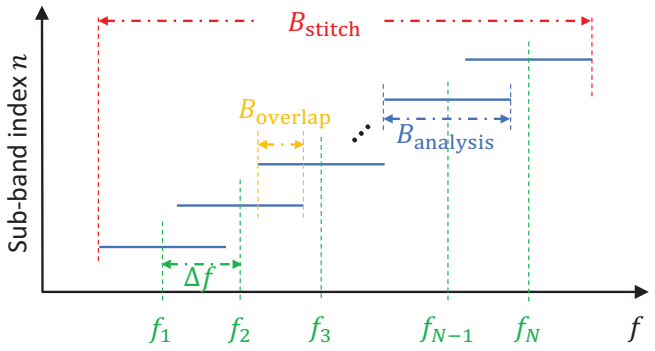

Fig. 2. Diagram of the relations among sub-bands. The nth sub-band is centered at f_n with the analysis bandwidth of B_{analysis}. The spacing between the center frequencies of adjacent sub-bands is Δf. The overlap bandwidth between adjacent sub-bands is B_{overlap}. The total stitched bandwidth is B_{stitch}.

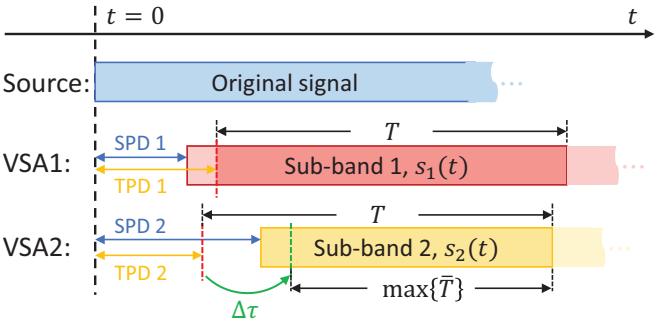

Fig. 3. Timing impairments between sub-bands with respect to the original signal for a two-band stitching scenario. The input signal arrives at each VSA after a sampling path delay (SPD). Each VSA starts recording after a triggering path delay (TPD), indicated with the red dashed line. The recording duration is T for both VSAs. The green dashed line indicates a virtual start of recording after delay $\Delta\tau$ correction. The recoverable duration of the data is $\bar{T}$ with a maximum value of $\max\{\bar{T}\} = T - |\Delta\tau|$.

band shall be about the same if noise is neglected. Recall that $H^{\text{analysis}}(f) \approx 1$ in the overlap band.

A. Timing impairment estimation

The timeline of the recording of two sub-band signals is given in Fig. 3. Consider the parallel setup in Fig. 1(b). Suppose a common trigger signal is sent to both VSAs. Due to potential different lengths of the sampling paths, triggering paths, or jitters, the starts of recording of the two VSAs (see Fig. 3) may not coincide at the same position relative to the beginning of their respective sub-band signals. This timing impairment from various sources can be summarized as a delay offset, $\Delta\tau$, between the recorded data of the two sub-bands.

Suppose both sub-bands are recorded for T seconds. Interpolate them to a target sampling rate B_{in}, which should be larger than or equal to the total bandwidth of the original input signal. Mix them to their IF center frequencies, i.e., $\pm\frac{1}{2}\Delta f$, respectively. Denote the resulting signals as $s_1(t)$ and $s_2(t)$ with $t \in [0, T]$. Convert them to the frequency domain using the discrete Fourier transform (DFT), and denote them as $S_1(f)$ and $S_2(f)$ with $f \in [-\frac{1}{2}B_{\text{in}}, \frac{1}{2}B_{\text{in}}]$.

An initial estimate of $\Delta\tau$, denoted as $\Delta\tau'$, is obtained through the circular cross-correlation of the two signals as (similar to [9])

$$\Delta\tau' = \arg\max_{\tau'} \left| \sum_{f \in f_{\text{overlap}}} S_1(f) S_2^*(f) e^{j2\pi f\tau'} \right|, \tag{3}$$

where $f_{\text{overlap}} = [-\frac{1}{2}B_{\text{overlap}}, \frac{1}{2}B_{\text{overlap}}]$, and $(\cdot)^*$ denotes the complex conjugate operator. Note that the applicability of (3) assumes the input signal has strong orthogonality in the time domain, e.g., pseudo-noise signals, so that a high peak can be found in the cross-correlation.

However, since the input signal could be arbitrary and recording is a causal process, circularly shifted data does not comply to the causality, and hence the estimate $\Delta\tau'$ from (3) might suffer from the artifacts due to circular shifting. Therefore, a refined estimation is further conducted to obtain a more accurate estimate based on the initial one.

To exclude the wrapped part of the signals from the estimation, we only consider the signals within a time window $[0, \bar{T}]$, where the theoretical maximum duration is $\max\{\bar{T}\} = T - |\Delta\tau|$. Since the true value of $\Delta\tau$ is unknown, we can use the initial estimate $\Delta\tau'$ in practice as a likely guess of $\max\{\bar{T}\}$. To cut the signals down to the time window, define

$$\bar{s}_1(t) = \sum_{f \in f_{B_{\text{in}}}} S_1(f) e^{j2\pi ft}, \tag{4}$$

$$\bar{s}_2(t; \Delta\tau' + \tau'') = \sum_{f \in f_{B_{\text{in}}}} S_2(f) e^{-j2\pi f(\Delta\tau' + \tau'')} e^{j2\pi ft}, \tag{5}$$

for $t \in [0, \bar{T}]$, where $f_{B_{\text{in}}} = [-\frac{1}{2}B_{\text{in}}, \frac{1}{2}B_{\text{in}}]$. Convert $\bar{s}_1(t)$ and $\bar{s}_2(t; \Delta\tau' + \tau'')$ to the frequency domain using DFT, and denote them as $\bar{S}_1(f)$ and $\bar{S}_2(f; \Delta\tau' + \tau'')$. The refined estimate is obtained as

$$\Delta\tau'' = \arg\min_{\tau''} \sigma \left(\angle \frac{\bar{S}_1(f)}{\bar{S}_2(f; \Delta\tau' + \tau'')} \right), \tag{6}$$

for $f \in f_{\text{overlap}}$, where $\angle(\cdot)$ evaluates phase angle at each frequency, and $\sigma(\cdot)$ evaluates the standard deviation over frequencies. The final estimate of the delay offset is $\Delta\tau = \Delta\tau' + \Delta\tau''$. As denoted in Fig. 3, correcting the timing of the recorded "sub-band 2" signal effectively pushes the real start of recording (red dashed line) to a virtual one (green dashed line) by $\Delta\tau$ in the recorded data.

The refined estimation is much more computationally expensive than the initial estimation, since it involves the (inverse) DFT for each search candidate of τ'' whereas the initial estimation computes only once (inverse) DFT for all τ'. However, knowing the initial estimate $\Delta\tau'$ helps to narrow down the search range for the second estimation significantly. In practice, the search range can be reduced to within several bins of the delay resolution, i.e., $1/B_{\text{in}}$. The resulting computational complexity can be found to be $O(M_{\tau''} N_t \log N_t)$ if the DFT is implemented with the fast Fourier transform (FFT), where $M_{\tau''}$ and N_t are the number of search candidates of τ'' and the number of recorded samples in the time duration T, respectively.

B. Magnitude and initial phase impairment estimation

The magnitude impairment $\Delta\alpha$ and the initial phase impairment $\Delta\phi$ can be estimated respectively as

$$\Delta\alpha = \left| \frac{1}{N_f} \sum_f \frac{\bar{S}_1(f)}{\bar{S}_2(f;\Delta\tau)} \right|, \tag{7}$$

$$\Delta\phi = \angle \left(\frac{1}{N_f} \sum_f \frac{\bar{S}_1(f)}{\bar{S}_2(f;\Delta\tau)} \right), \tag{8}$$

over the N_f frequency bins within $f \in f_{\text{overlap}}$. In the end, the final stitched signal in the frequency domain can be obtained as

$$\bar{Y}(f) = \begin{cases} \bar{S}_1(f), & -\frac{1}{2}B_{\text{in}} \le f < -\frac{1}{2}B_{\text{overlap}} \\ \bar{S}_1(f), & |f| \le \frac{1}{2}B_{\text{overlap}} \\ \bar{S}_2(f;\Delta\tau)\cdot\Delta\alpha e^{j\Delta\phi}, & \frac{1}{2}B_{\text{overlap}} < f \le \frac{1}{2}B_{\text{in}} \end{cases} \tag{9}$$

for $f \in f_{B_{\text{in}}}$. We can also obtain the time-domain stitched signal, $\bar{y}(t)$ for $t \in [0, \bar{T}]$, by computing the inverse DFT of $\bar{Y}(f)$. It is worth noting that the above calibration method can be used for general multi-band stitching scenarios by going through all adjacent sub-bands.

A summary of the procedure of the proposed band-stitching method is given below:

i) Measure the I/Q data of each sub-band, following (1) and (2).
ii) Interpolate the sub-band data to the bandwidth of the original input signal, e.g. by zero-padding in the frequency domain.
iii) Mix each sub-band to its respective IF center frequency, e.g. by multiplying a phasor in the time domain.
iv) Estimate and correct the delay offset $\Delta\tau$ between sub-bands, using (3) and (6).
v) Estimate and correct the magnitude and initial phase offset, $\Delta\alpha$ and $\Delta\phi$, between sub-bands, using (7) and (8).
vi) Calculate the final stitched data $\bar{Y}(f)$ and $\bar{y}(t)$, using (9).

It is worth noting that the above impairment correction method requires the presence of the original signal in the overlap band. Therefore, for signals with large gaps in the spectrum, e.g., due to carrier aggregation, the overlap band shall be assigned outside the gap region.

IV. Validation Measurements

A. Measurement description

We conducted two measurement series with the sequential setup, see Fig. 1(a), at 1 GHz and 28 GHz center frequency, respectively. The 28 GHz measurement was realized with additional external mixers.

For both measurement series, the same measurement instruments were used. On the transmitter side, a Rohde & Schwarz (R&S) SMBV100B was used as the signal generator. The baseband signal was chosen to be the "NR-FR1-TM3.1a-FDD-100MHz-30kHz" signal, which is an OFDM signal of quadrature amplitude modulation (QAM) of order 256 with

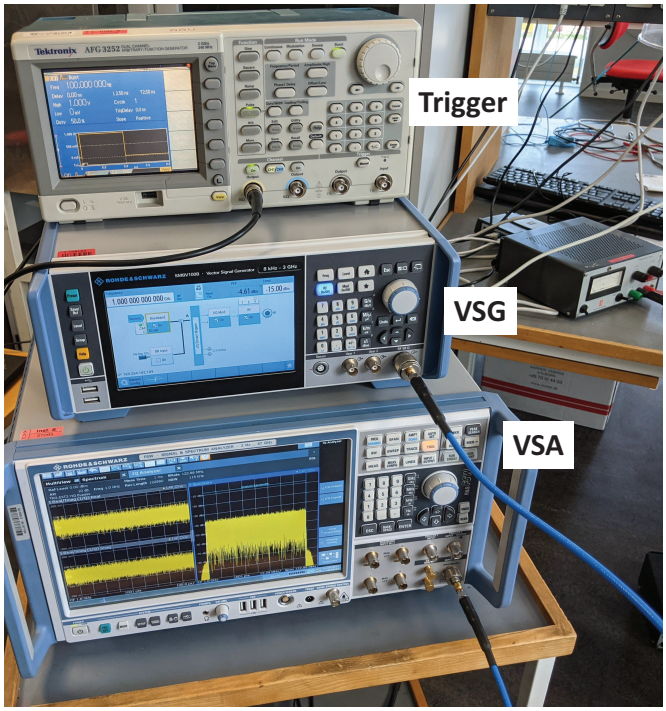

Fig. 4. Photo of the measurement setup of Series #1. Three measurement instruments are used: a vector signal generator (R&S SMBV100B), a vector signal analyzer (R&S FSW67), and a trigger signal generator (Tektronix AFG 3252).

100 MHz channel bandwidth and 30 kHz sub-carrier spacing [16]. A frame of the signal lasts for 10 ms, which consists of 20 slots. The signal generator was set to the "retrigger" mode, and it started to transmit the same frame continuously and repetitively once it received the trigger signal. On the receiver side, an R&S FSW67 was used as the VSA. It started recording the I/Q signal at its configured center frequency and sampling rate once it received the same trigger signal as for the signal generator for a configured recording duration. The signal generator and the VSA were locked to the same 10 MHz reference frequency during the measurement.

Besides different center frequencies, stitching with different numbers of sub-bands was also conducted, i.e., from one-band stitching (B1) to four-band stitching (B4) through varying the center frequency and sampling rate of each sub-band measurement at the VSA. Note that the one-band stitching case is the same as the conventional full-bandwidth measurement without band-stitching. All measurements were repeated three times.

A summary of the measurements conducted in the experiment is given in Table I, and the settings of the sub-band measurements for individual band-stitching cases are given in Table II. A photo of the measurement setup of Series #1 is shown in Fig. 4.

An example of the measured I/Q converted to the frequency domain is shown in Fig. 5 for the B1 and B3 cases of Series #1, i.e., the conventional full-bandwidth measurement case and the three-band stitching case. Each sub-band I/Q of the B3 case has been interpolated from its recording sampling rate, 62.5 MHz, to the target sampling rate 122.88 MHz, and further

TABLE I
GENERAL CONFIGURATIONS OF THE MEASUREMENT SERIES

Measurement series	Series #1	Series #2
Setup type	Sequential	Sequential
Center frequency	1 GHz	28 GHz[1]
Band-stitching case	B1[2], B2, B3, B4	B1[2], B2, B3, B4
Recording duration	60 ms	60 ms
Repetitions	3	3

1: with external mixers.
2: B1 denotes the conventional full-bandwidth measurement.

TABLE II
SETTINGS OF THE SUB-BAND MEASUREMENTS FOR THE FOUR BAND-STITCHING CASES

Band-stitching case		B1[1]	B2	B3	B4
Number of sub-bands (N)		1	2	3	4
Sampling rate [MHz]		122.88	100	62.5	50
IF center frequency per sub-band [MHz]	f_1	0	-30	-30	-30
	f_2	-	30	0	-10
	f_3	-	-	30	10
	f_4	-	-	-	30
B_{analysis} [MHz]		98.304	80	50	40
Δf [MHz]		0	60	30	20
B_{overlap} [MHz]		20	20	20	20
B_{stitch} [MHz]		98.304	140	110	100

1: B1 denotes the conventional full-bandwidth measurement.

mixed to their respective IF center frequencies, i.e., -30 MHz, 0 MHz, and 30 MHz. The small frequency components on the very left and right side of the "sub-band 1" and "sub-band 2" are caused by the anti-aliasing filter and decimation of the VSA while recording the I/Q data. We can see the envelopes of the three sub-bands, if superimposed, follow that of the B1 case within the channel bandwidth.

B. Impairment correction results

The same example (the B3 case of Series #1) showed in Fig. 5 is taken for the illustration. The impairment estimation and correction is done over the 20 MHz overlap frequency band between adjacent sub-band I/Q. The initial and refined delay between "sub-band 1" and "sub-band 2" are estimated to be $\Delta\tau' = 1 \cdot \delta_\tau$ and $\Delta\tau' = 0.03 \cdot \delta_\tau$ with $\delta_\tau = 1/122.88$ μs. Between "sub-band 2" and "sub-band 3", the delay estimates are $\Delta\tau' = 1 \cdot \delta_\tau$ and $\Delta\tau' = 0.18 \cdot \delta_\tau$. The phase alignment in the two overlap frequency bands are shown in Fig. 6 for the cases without delay correction, with the initial delay correction, and with the refined delay correction. We can see a clear improvement in the alignment with the initial delay correction and that of the refined delay correction seems marginal.

The initial phase offset is estimated from the phase alignment with the refined delay correction, and it is $\Delta\phi = 39.92°$ between "sub-band 1" and "sub-band 2" and $\Delta\phi = -74.83°$ between "sub-band 2" and "sub-band 3".

Similarly, the magnitude alignment in the two overlap frequency bands are shown in Fig. 7. No significant difference among the three cases is seen, which is reasonable since the estimated delay offsets between adjacent sub-bands are

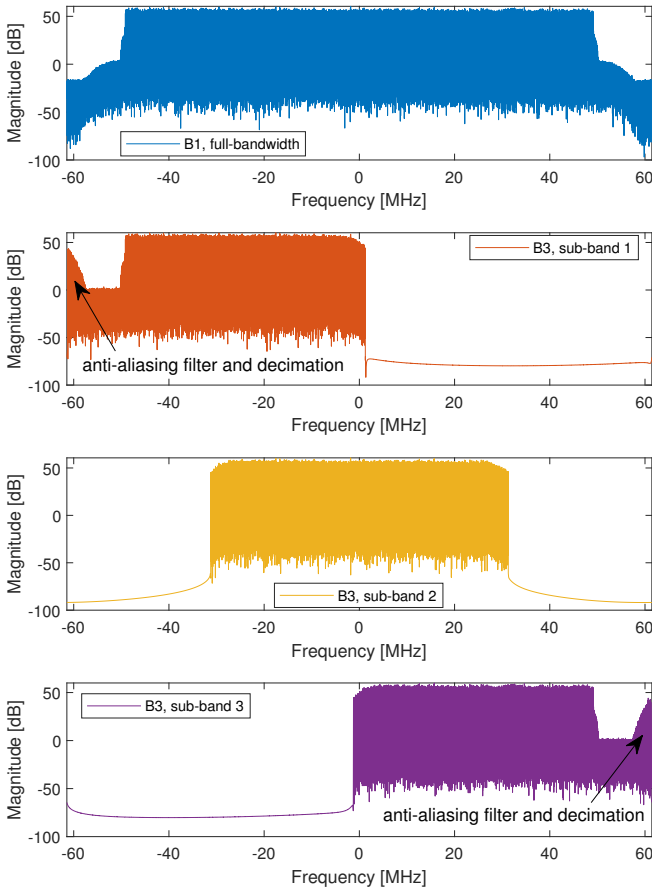

Fig. 5. The measured I/Q converted to the frequency domain. Each sub-band I/Q of the B3 case has been interpolated to 122.88 MHz sampling rate and mixed to their respective IF frequencies, i.e., -30 MHz, 0 Hz, and 30 MHz.

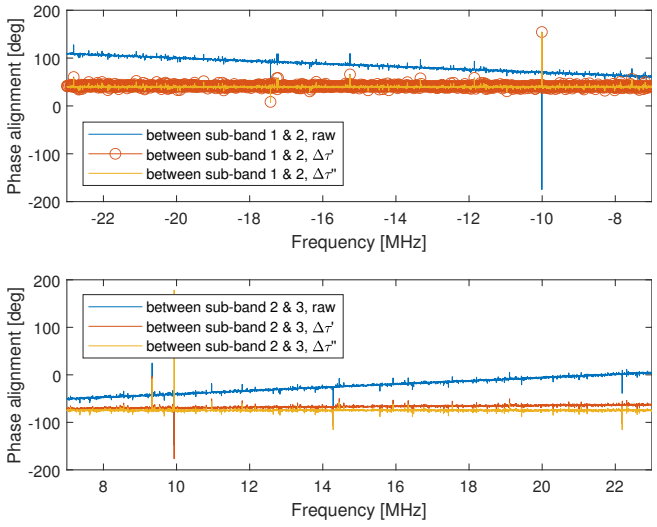

Fig. 6. The phase alignment in the overlap frequency band between the adjacent sub-band I/Q, i.e., (top) between "sub-band 1" and "sub-band 2", and (bottom) between "sub-band 2" and "sub-band 3". Three cases are shown, i.e., the phase alignment without any delay correction (raw), that with the initial delay correction ($\Delta\tau'$), and that with the refined delay correction ($\Delta\tau''$).

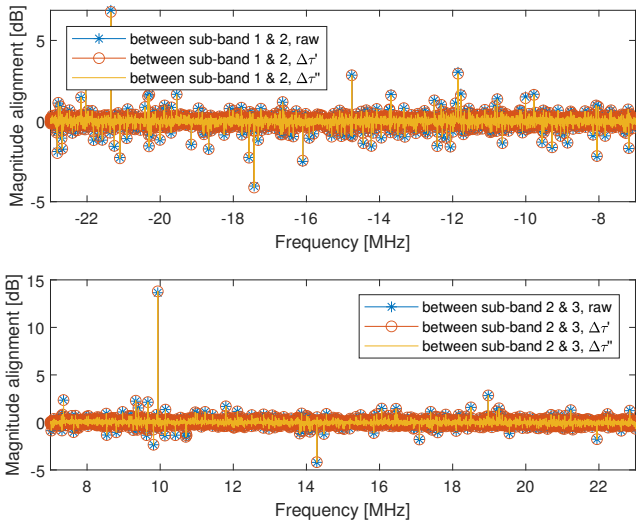

Fig. 7. The magnitude alignment in the overlap frequency band between the adjacent sub-band I/Q, i.e., (top) between "sub-band 1" and "sub-band 2", and (bottom) between "sub-band 2" and "sub-band 3". Three cases are shown, i.e., the magnitude alignment without any delay correction (raw), that with the initial delay correction ($\Delta\tau'$), and that with the refined delay correction ($\Delta\tau''$).

TABLE III
ESTIMATED OFFSETS FOR THE B3 CASE OF SERIES #1

		Rep. #1	Rep. #2	Rep. #3
Between sub-band 1 & 2	$\Delta\tau'$	$1 \cdot \delta_\tau$	$1 \cdot \delta_\tau$	$2 \cdot \delta_\tau$
	$\Delta\tau''$	$0.03 \cdot \delta_\tau$	$0.30 \cdot \delta_\tau$	$0.08 \cdot \delta_\tau$
	$\Delta\phi$	$39.92°$	$-17.56°$	$141.14°$
	$\Delta\alpha$	0.9986	0.9983	0.9984
Between sub-band 2 & 3	$\Delta\tau'$	$1 \cdot \delta_\tau$	$1 \cdot \delta_\tau$	$1 \cdot \delta_\tau$
	$\Delta\tau''$	$0.18 \cdot \delta_\tau$	$0.34 \cdot \delta_\tau$	$0.03 \cdot \delta_\tau$
	$\Delta\phi$	$-74.83°$	$-146.60°$	$-117.77°$
	$\Delta\alpha$	0.9995	0.9999	1.0002

1: $\delta_\tau = 1/122.88$ μs
2: Repetition (Rep.)

relatively small. The estimated magnitude offsets in the linear scale are $\Delta\alpha = 0.9986$ between "sub-band 1" and "sub-band 2" and $\Delta\alpha = 0.9995$ between "sub-band 2" and "sub-band 3", which indicates the magnitude offsets between the adjacent sub-bands are almost negligible.

A summary of the estimated delay, initial phase, and magnitude offsets for all three repetitions of the B3 case of Series #1 is given in Table III. We can see that the estimated delay offsets ($\Delta\tau'$ and $\Delta\tau''$) for all three repetitions remain relatively small, i.e., within two delay resolutions. Besides, an interesting observation is that the estimated initial phase offset $\Delta\phi$ changes over the repetitions under the condition that the signal generator and the VSA were locked to the same 10 MHz reference frequency during the measurement, which indicates that the impairment correction is probably needed every time a new band-stitching measurement is conducted.

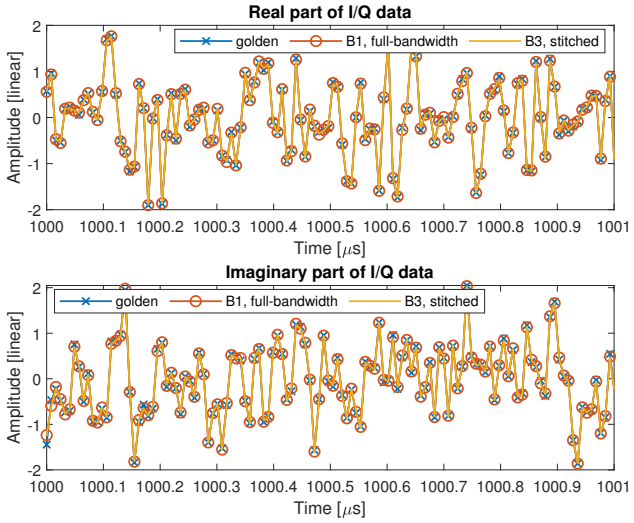

Fig. 8. (top) The real part and (bottom) the imaginary part of the golden I/Q data and that of the B1 and B3 cases, respectively. A 1-μs segment is shown.

C. Stitched I/Q data in the time and frequency domain

From the EVM evaluation point of view, it is specified in the standard [16] that the EVM is evaluated over a complete 1-frame signal from its frame head. Therefore, we stitch the I/Q data for a 2-frame duration to ensure that there exists at least one complete frame of the signal within the stitched duration. Moreover, we generate a frame of the golden I/Q data for the considered "NR-FR1-TM3.1a-FDD-100MHz-30kHz" signal according to the standard [16], [18].

Both the I/Q data of the B1 and B3 cases are time and power aligned to the golden I/Q data, and a segment of 1-μs duration of the aligned I/Q data is shown in Fig. 8 in terms of the real and the imaginary part, respectively. No significant differences among the three data sets are seen.

The I/Q data are further compared in the frequency domain, which is more important for OFDM signals, as shown in Fig. 9. Within the center 100 MHz channel bandwidth, both the B1 and B3 cases have a good match to the golden I/Q data, except for the frequency range around 40 MHz. Since the deviation happened in both the B1 and the B3 cases in the same way, it is probably caused by the signal generator that the original RF signal itself is slightly distorted in that frequency range.

The normalized root-mean-square error (NRMSE) is further calculated to quantitatively measure the deviation from the B1 and B3 cases to the golden data, respectively, within the center 100 MHz channel bandwidth. The NRMSE is defined as

$$\text{NRMSE}(a) = \frac{\sqrt{\text{mean}\left(|a(f) - b(f)|^2\right)}}{\sqrt{\text{mean}\left(|b(f)|^2\right)}} \times 100\%, \quad (10)$$

where $a(f)$ denotes the measured I/Q data in the frequency domain, and $b(f)$ denotes the golden I/Q data in the frequency domain. The $\text{mean}(\cdot)$ is evaluated over the frequency samples within the center 100 MHz signal bandwidth. The resultant

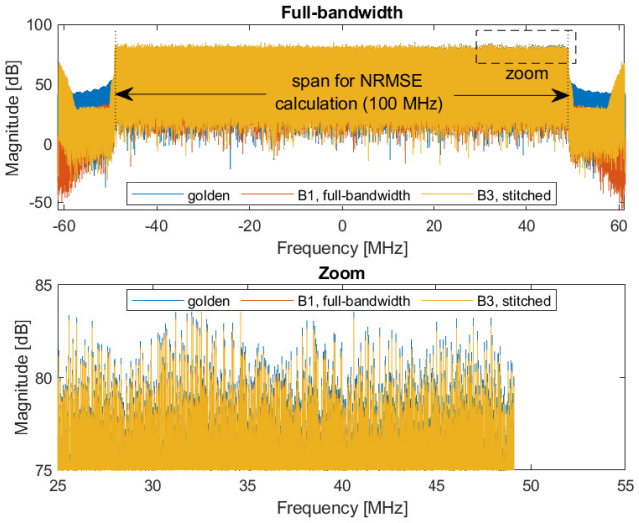

Fig. 9. The frequency-domain counterpart of the golden I/Q data and that of the B1 and B3 cases, respectively, (top) over the full 122.88 MHz band and (bottom) that zoomed to the frequency range around 40 MHz where a slight deviation is observed.

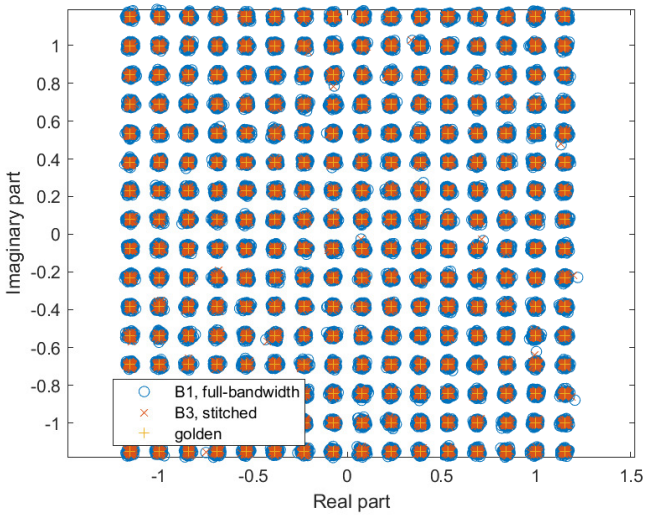

Fig. 10. The constellation of the demodulated symbols of the first slot in the PDSCH channel for the golden I/Q data and that of the B1 and B3 cases, respectively. The averaged EVM of the whole frame is 1.31% for the B1 case and 0.97% for the B3 case.

TABLE IV
NRMSE OF ALL MEASUREMENTS WITH RESPECT TO THE GOLDEN DATA

		Rep. #1	Rep. #2	Rep. #3
Series #1	B1	3.23%	3.30%	3.26%
	B2	3.60%	3.59%	3.60%
	B3	3.78%	3.73%	3.74%
	B4	4.24%	4.25%	4.29%
Series #2	B1	2.06%	2.02%	2.05%
	B2	1.96%	2.15%	1.99%
	B3	2.47%	2.39%	2.53%
	B4	1.92%	1.96%	2.02%

1: Repetition (Rep.)

TABLE V
AVERAGED EVM OF ALL MEASUREMENTS WITH RESPECT TO THE GOLDEN DATA

		Rep. #1	Rep. #2	Rep. #3
Series #1	B1	1.31%	1.31%	1.30%
	B2	0.97%	0.98%	0.97%
	B3	0.97%	0.97%	0.96%
	B4	0.96%	0.96%	0.96%
Series #2	B1	1.09%	1.09%	1.11%
	B2	1.00%	1.02%	1.01%
	B3	1.01%	1.02%	1.01%
	B4	1.00%	1.02%	1.01%

1: Repetition (Rep.)

NRMSE for the B1 case and the B3 case is 3.32% and 3.78%, respectively.

A summary of the resultant NRMSE for all measurements is given in Table IV. We can see that the NRMSEs are stable across the three repetitions. Taking the values of the B1 case, i.e., the conventional full-bandwidth measurement, as the reference, the B4 case results in the largest difference of about 1% for Series #1, and the B3 case results in the largest difference of about 0.5% for Series #2.

D. Demodulation and EVM

An in-house demodulation and EVM evaluation algorithm is implemented according to the standard [16]. Given the known golden data, the frame head is found and the carrier recovery is conducted. Given the known frame structure, the symbols are further demodulated. Moreover, equalization is performed with respect to the demodulation reference signal (DMRS) symbols. Lastly, the EVM is calculated for each slot within the frame over the symbols in the physical downlink shared channel (PDSCH).

The constellation of the demodulated symbols of the first slot in the PDSCH channel is shown in Fig. 10 for the golden I/Q data and that of the B1 and B3 cases, respectively. The root-mean-square averaged EVM is calculated over the individual EVMs of the 20 slots within the frame to represent the EVM of the whole frame. The resultant averaged EVM for the B1 and B3 cases are 1.31% and 0.97%, respectively.

A summary of the resultant averaged EVM for all measurements is given in Table V. We can see that the averaged EMV are stable across the three repetitions. Taking the values of the B1 case, i.e., the conventional full-bandwidth measurement, as the reference, all the band-stitched results (from B2 to B4) seem to be lower than the reference values by about 0.3% in Series #1, whereas no significant differences between the band-stitched results and the reference values are seen in Series #2.

The power spectrum density of the I/Q data is calculated with the Welch method [19] for all band-stitching cases and measurement series as shown in Fig. 11. A difference of about 2 dB in the noise power density is seen between the full-bandwidth B1 case and the stitched B2-B4 cases in Series #1, whereas no significant difference is seen in Series #2. The difference in the resultant averaged EVM is likely caused by

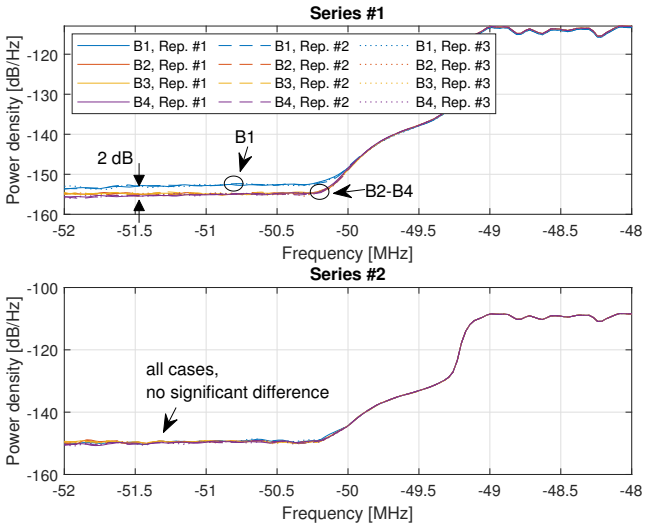

Fig. 11. The power spectrum density of all band-stitching cases and measurement series around −50 MHz frequency where the transition between the signal and noise occurs. A difference of about 2 dB in the noise density is seen between the full-bandwidth B1 cases and the stitched B2-B4 cases in Series #1, whereas no significant difference is seen for all cases in Series #2.

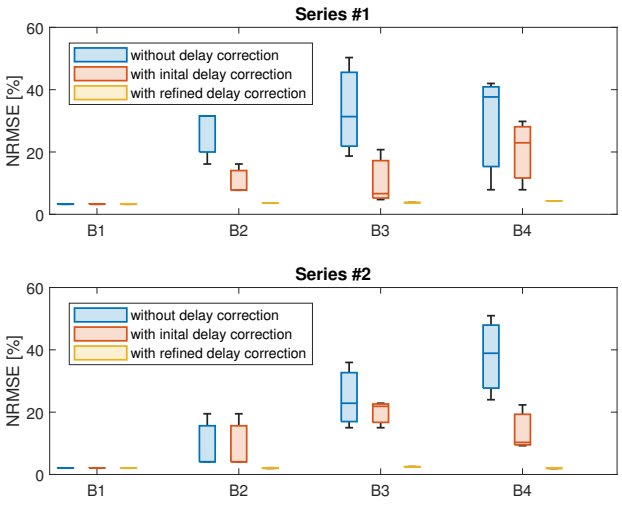

Fig. 12. The effect of the two-step delay correction method in the NRMSE for all band-stitching cases and measurement series. The central mark of the box denotes the median, and the top and bottom edges of the box denote the 75th and 25th percentiles, respectively. The tips of the top and the bottom whiskers indicate the maximum and minimum values, respectively. The statistics are derived from the three repetitions.

the change of signal-to-noise ratio in Series #1.

From a separate stand-alone noise measurement of the VSA, we find the VSA might switch its internal sampling paths depending on the configured sampling rate with 100 MHz as a threshold, above which the noise power density increases by about 2 dB. This difference coincides with the observation in Series #1 of Fig. 11. As for Series #2, the effect of the change of noise power density from different sampling rates is obscured by the extra noise from the external mixers.

Lastly, the effect of the two-step delay correction method is shown in Fig. 12 and Fig. 13 in terms of the NRMSE and the averaged EVM, respectively. Three cases are compared, namely without delay correction, with initial delay correction, and with refined delay correction. The first case is equivalent to timing alignment only with common trigger signals, and zero delay offset is applied to the raw sub-band I/Q data before the stitching. The second case is equivalent to timing alignment with both the triggering and the cross-correlation, and the estimated initial delay offset is applied before the stitching. In the third case, both the estimated initial and refined delay offset is applied before the stitching. Note that the initial phase and magnitude offset correction are always conducted in all three cases under their respective delay offset conditions. Therefore, the only variable among the three cases is the delay offset to be corrected.

The statistics are computed from the three repetitions for each case, and presented in the box plot. The central mark of the box denotes the median, and the top and bottom edges of the box denote the 75th and 25th percentiles, respectively. The tips of the top and the bottom whiskers indicate the maximum and minimum values, respectively.

For the NRMSE in Fig. 12, within each band-stitching case (B2, B3, or B4), the spread of the boxes, i.e., the difference between the maximum and the minimum, decreases as the

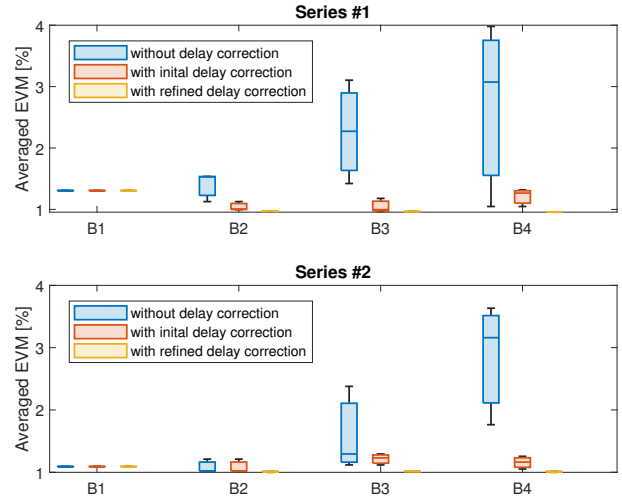

Fig. 13. The effect of the two-step delay correction method in the averaged EVM for all band-stitching cases and measurement series. The central mark of the box denotes the median, and the top and bottom edges of the box denote the 75th and 25th percentiles, respectively. The tips of the top and the bottom whiskers indicate the maximum and minimum values, respectively. The statistics are derived from the three repetitions.

initial and refined delay correction are conducted, and the level of the box converges to that of the B1 case. It is also worth mentioning that, in the case of the "without delay correction" (blue boxes), the spread of the box increases with the number of sub-bands that are stitched (from B2 to B4). This is reasonable since the more sub-bands to be stitched, the more impairments are left untreated in this case. A similar behavior is seen for the averaged EVM in Fig. 13.

V. Conclusion

In this paper, we discussed how to use band-stitching for wideband vector measurements with VSAs of insufficient analysis bandwidth. We proposed a two-step delay estimation method to correct the timing impairment between adjacent sub-bands in post-processing based on the recorded sub-band data. The method was assessed with two series of validation measurements for the sequential setup at 1 GHz and 28 GHz center frequencies, respectively. The results from three band-stitching scenarios, i.e., two-band stitching, three-band stitching, and four-band stitching, were compared in terms of the NRMSE and the averaged EVM. Excellent consistency between the stitched I/Q data and the reference I/Q data has been seen, which indicates the proposed sub-band impairment estimation method works well. Moreover, the significance of conducting the second refined delay correction has also been demonstrated by comparing the resultant NRMSE and averaged EVM to that of the state-of-the-art methods, i.e., timing alignment through common trigger signals and through the cross-correlation.

The band-stitching process with the proposed sub-band correction method allows for measurement of signals of wider bandwidth than the intrinsic analysis bandwidth of VSAs. Potential applications may include ultra-wideband signals, THz communication, spectral leakage measurement of power amplifiers, etc. The whole process can be implemented with software defined radios as well with a high flexibility.

Compared to the traditional vector measurement with a single VSA where all measures are reported at once without much user intervention, additional computational complexity is introduced in the post-processing for sub-band correction in exchange of the effectively extended analysis bandwidth. In future work, an extensive measurement uncertainty analysis needs to be investigated to quantify more thoroughly the accuracy of the whole measurement process for, e.g., various types of test signals and a larger number of stitched bands.

Acknowledgment

The authors would like to thank Mr. Huaqiang Gao, Mr. Kristian Bank, and Mr. Kim Olesen, for their help with the practical measurements.

References

[1] *NR; Base Station (BS) radio transmission and reception*, 3rd Generation Partnership Project Std. 3GPP TS 38.104, Rev. V15.2.0, 2019.

[2] W. C. Black and D. A. Hodges, "Time interleaved converter arrays," *IEEE Journal of Solid-State Circuits*, vol. 15, no. 6, pp. 1022–1029, 1980.

[3] M. Seo, M. Rodwell, and U. Madhow, "Comprehensive digital correction of mismatch errors for a 400-Msamples/s 80-dB SFDR time-interleaved analog-to-digital converter," *IEEE Transactions on Microwave Theory and Techniques*, vol. 53, no. 3, pp. 1072–1082, 2005.

[4] S. R. Velazquez, T. Q. Nguyen, and S. R. Broadstone, "Design of hybrid filter banks for analog/digital conversion," *IEEE Transactions on Signal Processing*, vol. 46, no. 4, pp. 956–967, 1998.

[5] S. L. Dark and C. N. White, "Time sequenced spectral stitching," Patent WO 2018/045 201 A1, 2018.

[6] E. M. Barich, "Method and system for performing vector spectral measurements of a radio frequency (RF) signal having a repetitive waveform," Patent US 9,851,383 B1, 2017.

[7] S. L. Dark, D. J. Baker, and J. R. Ammerman, "Spectral stitching method to increase instantaneous bandwidth in vector signal analyzers," Patent US 9,326,174 B1, 2016.

[8] G. Feldhaus, A. Roth, and M. Ruengeler, "Test and measurement device, method for calibrating a test and measurement device as well as method for analyzing a high bandwidth of a radio frequency signal," Patent US 10,436,826 B2, 2019.

[9] D. Wisell, D. Rönnow, and P. Händel, "A technique to extend the bandwidth of an RF power amplifier test bed," *IEEE Transactions on Instrumentation and Measurement*, vol. 56, no. 4, pp. 1488–1494, 2007.

[10] K. A. Remley, D. F. Williams, D. Schreurs, and M. Myslinski, "Measurement bandwidth extension using multisine signals: Propagation of error," *IEEE Transactions on Microwave Theory and Techniques*, vol. 58, no. 2, pp. 458–467, 2010.

[11] C. U. Bas, V. Kristem, R. Wang, and A. F. Molisch, "Real-Time Ultra-Wideband Channel Sounder Design for 3-18 GHz," *IEEE Transactions on Communications*, vol. 67, no. 4, pp. 2995–3008, 2019.

[12] W. Fan, P. Kyosti, L. Hentila, and G. F. Pedersen, "A flexible millimeter-wave radio channel emulator design with experimental validations," *IEEE Transactions on Antennas and Propagation*, vol. 66, no. 11, pp. 6446–6451, 2018.

[13] J. Cao, F. Tila, and A. Nix, "Design and implementation of a wideband channel emulation platform for 5G mmWave vehicular communication," *IET Communications*, vol. 14, no. 14, pp. 2369–2376, 2020.

[14] Y. Ji, W. Fan, and G. F. Pedersen, "Wideband radio channel emulation using band-stitching schemes," in *14th European Conference on Antennas and Propagation (EuCAP)*, 2020, pp. 1–5.

[15] L. Wen, , Z. Wang, L. Zhang, Q. Yuan, C. Ge, and T. Yang, "Frequency quasi-linear swept light source based on multi-frequency time-matched spectrum stitching," *IEEE Photonics Journal*, vol. 12, no. 6, 2020.

[16] *NR; Base Station (BS) conformance testing Part 1: Conducted conformance testing*, 3rd Generation Partnership Project Std. 3GPP TS 38.141-1, Rev. V16.1.0, 2019.

[17] Rohde & Schwarz, *R&S FSW I/Q Analyzer and I/Q Input Interfaces User Manual*.

[18] *NR; Physical channels and modulation*, 3rd Generation Partnership Project Std. 3GPP TS 38.211, Rev. V16.6.0, 2021.

[19] P. D. Welch, "The Use of Fast Fourier Transform for the Estimation of Power Spectra: A Method Based on Time Averaging Over Short, Modified Periodograms," *IEEE Transactions on Audio and Electroacoustics*, vol. 15, no. 2, pp. 70–73, 1967.

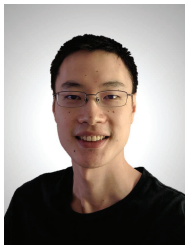

Yilin Ji received his B.Sc. degree in Electronics Science and Technology and M.Eng degree in Integrated Circuit Engineering from Tongji University, China, in 2013 and 2016, respectively. In 2021, he received his Ph.D. degree in Wireless Communications from Aalborg University, Denmark. He is currently a Postdoc at the Antennas, Propagation and Millimeter-wave Systems (APMS) Section at Aalborg University, Denmark. His main research areas are propagation channel characterization, and MIMO over-the-air testing.

Jesper Ødum Nielsen received his master's degree in electronics engineering in 1994 and a PhD degree in 1997, both from Aalborg University, Denmark. He is currently employed at Department of Electronic Systems at Aalborg University, Denmark, in the Antennas, Propagation and Millimeter-wave Systems section. His main areas of interests are experimental investigation of the mobile radio channel and the influence mobile device users have on the channel. Among other things, he has been involved in Massive MIMO and mm-wave channel sounding and modeling, as well as measurements using live LTE networks. In addition he has been working with radio performance evaluation, including over the air testing of active wireless devices.

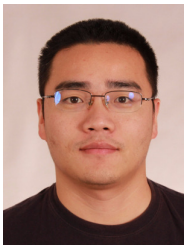

Wei Fan received his Bachelor of Engineering degree from Harbin Institute of Technology, China, in 2009, Master's double degree with highest honours from Politecnico di Torino, Italy, and Grenoble Institute of Technology, France, in 2011, and Ph.D. degree from Aalborg University, Denmark, in 2014. From February 2011 to August 2011, he was with Intel Mobile Communications, Denmark, as a Research Intern. He conducted a three-month internship at Anite telecoms oy, Finland, in 2014. He is currently an Associate Professor at the Antennas, Propagation and Millimeter-wave Systems (APMS) Section at Aalborg University. His main areas of research are over-the-air testing of multiple-antenna systems, radio channel sounding, modelling and emulation.